

Nitric Oxide Pathways in Surface-Flame Radiant Burners

M.D. Rumminger* and R.W. Dibble

Department of Mechanical Engineering, University of California, Berkeley, CA 94720-1740, USA

Abstract

Nitrogen oxide (NO_x) formation in surface-flame burners is studied. Surface-flame burners are typically made of metal fibers, ceramic fibers, or ceramic foam and provide radiant flux with low pollutant emissions. A one-dimensional model represents combustion on and within the porous medium using multistep chemistry, separate gas and energy equations, and a radiatively participating porous medium. We describe experimental measurements of NO_x profiles above a surface-flame burner and compare them to model predictions. The model predicts NO_x concentration with reasonable success. Deviations between model and experiment are primarily the result of heat loss in the experiment that is not considered in the model. Reaction rate analysis is performed to identify the chemical kinetic source of NO in the flame. Zeldovich NO is significant only at the highest firing rate studied (600 kW/m^2 , $\phi = 0.9$), where it is responsible for 50-60% of the total NO. At the lower firing rates (200 and 300 kW/m^2 , $\phi = 0.9$), where total NO is low, nearly all of the NO is formed in the flame front. Zeldovich NO accounts for 20-30% percent of the total NO, the Fenimore pathway accounts for less than 10% of the NO, and 50-75% percent of the NO is formed through the NNH, N_2O and other paths. Sensitivity analysis shows that NO production in the flame front is most sensitive to $\text{NNH} + \text{O} = \text{NH} + \text{NO}$, with $\text{CH} + \text{N}_2 = \text{HCN} + \text{N}$ having the second highest sensitivity coefficient. At the lower firing rates NO emission is insensitive to porous medium properties, while at the high firing rate NO emission is slightly sensitive to porous medium properties.

Introduction

As infrared heating becomes increasingly widespread in industries such as paper manufacturing and food processing, the role of the gas-fired radiant heaters will become more important because they have many advantages over electric heaters [1, 2]. Porous direct-fired surface-flame burners stabilize a premixed flame on the surface of an inert porous medium and typically burn premixed natural gas with air at lean equivalence ratios. These burners are used as a source of radiant energy or as a stable low- NO_x premixed burner. In 'radiant mode', which occurs at low flow rates, the burner surface glows uniformly. As the flow rate increases, part or all of the flame will lift from the porous medium, which is called the 'blue-flame mode'. Understanding of interactions between premixed flames and porous media will enable design of radiant burners with higher radiant efficiency, wider operating range and lower pollutant emission. As nitrogen oxide

($\text{NO}_x \equiv \text{NO} + \text{NO}_2$) regulations become more stringent, design of gas burners with minimal NO_x emissions will be critical.

Models of combustion in porous media have been steadily improving. Early studies, such as Singh et al. [3] and Andersen [4] approximated the flame with a heat release function (e.g., a delta function). Other models have employed a one-step chemical mechanism [5, 6]. Bouma et al. [7] used a skeletal methane mechanism without nitrogen chemistry and then used a post-processor to calculate the nitrogen species in a blue-flame-mode ceramic foam burner. Models that employ multistep chemistry have also been used to study burners that are significantly different than the burners in this study [8, 9]. Sullivan and Kendall [10] modeled the gas downstream of the burner surface with multistep kinetics and analyzed the NO_x formation mechanism with some success. They found that prompt NO_x formation depended heavily on equivalence ratio, while thermal NO_x formation depended heavily on flow rate.

* Corresponding author. E-mail: mrumminger@gmail.com

Despite their success, the model is not suitable for analyzing the effect of burner properties on performance, because heat transfer in the porous medium is not considered.

Williams et al. [11] made extensive measurements on a cylindrical-shaped surface-flame burner with a ceramic fiber porous medium that was operating in radiant mode. The measurements included gas temperature, radiant efficiency (percent of chemical input that is emitted as thermal radiation), surface temperature, major species profiles and NO_x profiles. From their experimental measurements and chemical kinetic estimates, they concluded that Fenimore NO_x was the most important pathway in radiant mode at firing rates of around 300 kW/m^2 (for lean ϕ). Note that we define the firing rate as the product of the methane mass fraction, the methane higher heating value and total gas flow rate per unit area. Thus, a change in firing rate changes the mass flow rate while holding ϕ constant.

Mokhov and Levinsky [12] measured NO concentrations above a laminar premixed burner-stabilized natural-gas/air flame to determine the effect of upstream heat loss on NO formation. They modeled the flame chemistry using a mechanism from Miller and Bowman [13] but did not examine the NO formation pathways in detail. They argued that there are lower limits to NO emission from natural gas burners, an important contribution to the debate on emission regulations.

Our overall research goal is to design a premixed porous burner that has low NO_x emissions, low CO emissions, a wide operating range and high radiant efficiency. Since burner performance is influenced by numerous parameters – such as porosity, extinction coefficient, burner thickness, effective solid thermal conductivity, pore size, and fiber size – a model is an essential research and development tool. By themselves, experimental parametric studies are impractical because of the innumerable permutations possible. A numerical model can guide experimental efforts and aid interpretation of experimental results. In this work, we focus on surface-flame burners that consist of one porous layer with homogeneous properties throughout. This paper uncovers the most important mechanisms of NO_x formation in surface-flame burners and explores whether fundamental performance limits may exist. We numerically and experimentally investigate NO_x formation in surface-flame burners operating in radiant and blue-flame mode and present NO_x profiles that show the chemical kinetic source of the NO_x . The model points to methods to reduce NO_x levels in current burners.

Model Description

We represent a surface-flame burner with a one-dimensional model. The model includes separate energy equations for the gas and solid, multistep chemistry, a domain that allows more accurate calculation of boundary temperatures, a user-definable flow rate, and a radiatively participating porous medium. We use the two-flux approximation for the radiative heat transfer. We do not fix the flame position but allow it to move as input conditions and burner properties change, thus allowing simulation of radiant or blue-flame mode. However, because the model assumes a perfect one-dimensional flow field, it cannot determine when the flame begins to lift from a portion of the burner, which is caused by inhomogeneity in the flow field or porous medium. Our model was influenced by the pioneering work of Sathe et al. [6] and Singh et al. [3]. The code is an extension of Sandia National Laboratory's one-dimensional premixed flame code by Kee et al. [14].

We assume the flame is one-dimensional and laminar; the gas is optically thin and ideal; combustion occurs at constant pressure; the porous medium is spectrally gray; and the porous medium is a hemispherically isotropic scatterer. Governing equations can be found in Rumminger et al. [15] or Rumminger [16].

In the model, combustion of premixed fuel and air occurs in an adiabatic, infinite duct that contains a porous medium. Figure 1 shows the computational domain for the model. Fuel and air enter an adiabatic, infinite duct at the left ($x = x_{in}$), flow into the porous medium (which extends from $x = 0$ to $x = L$) and exit at $x = x_{out}$ after reacting.

The computational domain used in this formulation is unlike the domain in any of the numerical studies cited above, except for Sathe et al. [6]. The boundary conditions for the gas are evaluated at the inlet and exit of the system – x_{in} and x_{out} in Fig. 1 – and the solid energy and radiative transfer boundary conditions are evaluated at $x = 0$ and $x = L$, points that are *between* the gas end points. The evaluation of gas and solid boundary conditions at different points allows less ambiguous definition of gas-phase boundary conditions, because a significant fraction of the heat release (and chemical reactions) can occur downstream of the burner surface ($x > L$) [11]. When we apply the zero-gradient downstream boundary condition at $x = x_{out}$ to the gaseous species, we ensure that x_{out} is far enough downstream so that most of the reactions have been completed. The gas boundary condition is evaluated at least 15 cm downstream of the porous medium in the simulations.

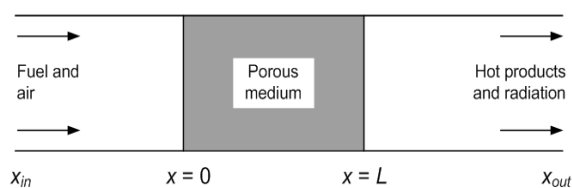


Fig. 1. Computational domain for radiant burner model. $x = 0$ and $x = L$ are the edges of the porous medium (shaded region). The upper and lower boundary lines are shown for clarity, but the actual boundaries are at $+\infty$ and $-\infty$.

Computational Methods

We use the *Chemkin* subroutines for chemical kinetics management [17] and the *Transport* package [18] to calculate gas properties. We find steady-state solutions with a modified-damped Newton-Raphson method, *Twopnt* [19], on *DEC Alpha* workstations. Solution time depends strongly on the initial guess and varies from several minutes to several hours. The solver uses an adaptive gridding technique and solutions typically contain 100-150 grid points. For numerical convergence, we specify an absolute tolerance of 10^{-10} and a relative tolerance of 10^{-5} .

Properties of the Porous Medium

Numerous porous medium properties determine the performance of a radiant burner: burner thickness, extinction coefficient, scattering albedo, effective thermal conductivity, forward scattering fraction, and the convective heat transfer coefficient. The extinction coefficient determines how strongly radiant energy is absorbed or scattered by the porous medium; it is the sum of the scattering coefficient and the absorption coefficient. The scattering albedo is the ratio of the scattering coefficient to the extinction coefficient; it is a measure of the fraction of radiant energy that is extinguished through scattering. The thermal conductivity used for the porous medium is an effective thermal conductivity, which depends on the material and the structure of the porous medium. The forward scattering fraction is an asymmetry parameter for the radiant heat transfer model and denotes the fraction of scattered radiation that scatters in the forward direction. The convective heat transfer coefficient is used for heat transfer between the gas and porous medium. The fiber burner in this study is fabricated from 22-micron diameter fibers of a high-temperature alloy (Fecralloy) with a porosity of 80% [20]. The convection coefficient within a metal fiber matrix comes from measurements by Golombok et al. [20]. In the correlation, the Reynolds number is based on fiber diameter ($Re = \dot{m}'' d/\mu$) and the Nusselt number (Nu) is

based on a unit area formulation ($Nu = h_o d/kg$) and the fiber diameter. For $Re < 0.4$ the correlation is $Nu = 0.04 Re^{0.53}$, and for $Re > 0.4$ the correlation is $Nu = 0.10 Re^{1.64}$. The following equation from [20] is used to convert from area-based convection coefficient to volumetric convection coefficient:

$$h_v = \frac{4 Nu k_g (1 - \epsilon)}{d^2} \quad (1)$$

We used reasonable estimates for the following properties: an extinction coefficient of 1000 m^{-1} ; a scattering albedo of 0.7; and a forward scattering fraction of 0.65. The estimates are based on properties used in other radiant burner models [8, 20] and extrapolations from experimental measurements of properties of other porous media [21]. We intended to use Mantle and Chang's [20] effective thermal conductivity correlation for sintered metal fibers, which relates the effective thermal conductivity of the porous medium to porosity, thermal conductivity of the gas, and thermal conductivity of the solid. The correlation is based on measurements made between 15 and 30 °C [23]. However, when we used the correlation with a bulk solid thermal conductivity of 10.0 W/m-K, simulations resulted in surface temperatures that were too low compared to previously published surface temperature measurements [24]. We speculate that the large temperature gradient ($\sim 400 \text{ K/mm}$) in the porous medium and thermal expansion of the fibers cause a reduction in the fiber-to-fiber sintering, which leads to a reduction in conduction. To more closely match experimental measurements of surface temperature [24], we use an effective thermal conductivity that is ten times lower than the result from Mantle and Chang's correlation. The thermal conductivity of the gas is calculated using subroutines from the *Transport* package [18]. The effective thermal conductivity of the gas inside the porous medium is modeled with a dispersion relation from Yagi et al. [25].

Reaction Rate Analysis

We use the GRI-Mech 2.11 [26] chemical mechanism for methane combustion, which includes nitrogen chemistry and consists of 49 species and 279 reactions. In our reaction rate analysis we consider the following NO formation mechanisms:

1. The extended Zeldovich mechanism [27], $N_2 + O \leftrightarrow N + NO$, $O_2 + N \leftrightarrow NO + O$, $N + OH \leftrightarrow NO + H$;
2. The Fenimore pathway [28], which is initiated by $CH + N_2 \leftrightarrow HCN + N$;
3. The N_2O mechanism [29, 30], $NH + NO \leftrightarrow N_2O + H$, $NCO + NO \leftrightarrow N_2O + CO$; and $N_2O + O \leftrightarrow 2NO$;

4. The NNH mechanism [31], $\text{NNH} + \text{O} \leftrightarrow \text{NH} + \text{NO}$;
5. The remaining reactions in the mechanism that produce NO.

At the pressure and temperatures considered in this paper, reactions involving interconversion of NO_2 to NO are unimportant because formation of one NO_2 molecule results in the removal of one NO molecule. The NO_2 is rapidly converted back to NO, resulting in no net change in the NO concentration. At high pressure or in combustors with rapid quenching (such as gas turbines), however, the re-conversion of NO_2 to NO can be incomplete, which results in elevated concentrations of NO_2 [32]. In the surface-flame burner studied here, NO_2 emissions are insignificant; nearly all of the NO_x is NO.

The contribution from each NO mechanism was found by reaction rate analysis, as in Schlegel et al. [33]. The NO production rate for each mechanism was calculated and then the production rate was numerically integrated to obtain an axial NO profile. The result was then multiplied by the molecular mass of NO and divided by mass flow rate per unit area, thus

$$[\text{NO}]_i(x) = \frac{M_{\text{NO}}}{\dot{m}''} \int_0^x \dot{\omega}_i'' dz \quad (2)$$

where $[\text{NO}]_i(x)$ is the mole fraction of NO from the i -th mechanism at location x , M_{NO} is the molecular mass of NO, \dot{m}'' is the mass flow rate per unit area (g/s-cm^2) and $\dot{\omega}_i''$ is the reaction rate (mol/s-cm^3) for the i -th NO mechanism. The contribution of N-atoms from the Fenimore pathway was calculated by determining the fraction of N atoms created by $\text{CH} + \text{N}_2 \leftrightarrow \text{HCN} + \text{N}$ and by the HCN to NCO to NH to N pathway, which Miller and Bowman [13] describe as the primary pathway for NO formation through the $\text{CH} + \text{N}_2$ reaction.

Experimental Measurements of NO_x

We experimentally measured NO_x profiles above a surface-flame burner with a porous medium that was made of sintered metal-fibers. A 2.2-mm thick, 152-mm square metal-fiber porous medium was glued into a housing that was filled with glass beads to ensure a uniform flow to the burner. The burner was mounted on an up-down translation stage. The burner radiated to the room and the gases cooled naturally. Natural gas (about 95% CH_4) was metered with a calibrated rotometer and air was metered with a sonic-orifice flow meter.

Exhaust gases were sampled above the center of the burner using a vertical uncooled low-aspect-ratio quartz probe with a orifice diameter of 0.6 mm and an expansion ratio of 4.3 inside the probe. The

sample-collection pump was sufficiently large to ensure sonic conditions in the probe. After a short passage (~ 30 cm) through stainless steel tubing, the sample entered a heated line that was maintained at 80°C to prevent water from condensing in the line before the water trap. The sample entered an ice bath for water removal and then entered the analyzer. We used a Horiba Chemiluminescent NO_x -analyzer with ranges of 0-10 ppm and 0-30 ppm; the span gas was 9.4 ± 0.47 ppm NO_x . O_2 was measured with a Horiba magneto-pneumatic analyzer; CO_2 was measured with a Horiba infrared analyzer (Disclaimer: mention of company names does not imply endorsement). The uncertainty of the NO_x measurements are based on the manufacturer's uncertainty specifications and the uncertainty of the span gas calibration. The uncertainty of each NO_x measurement depends on the range setting of the analyzer and the measured NO_x concentration, so the magnitude of each error bar in Fig. 2 and Fig. 3 is slightly different. The overall uncertainty is approximately $\pm 6\%$.

We measured NO_x , O_2 , and CO_2 concentrations for three firing rates (200, 300, and 600 kW/m^2) at $\phi = 0.9$ and two firing rates (200, 300 kW/m^2) at $\phi = 0.8$. At the lower firing rates the burner was operating in radiant mode, but at 600 kW/m^2 the flame was slightly lifted around the edges of the metal fiber porous medium and thus technically a blue-flame burner. Calculated flame temperature and radiant efficiency for each condition can be found in Table 1. All measurements were made for total NO_x to avoid concerns about conversion of NO to NO_2 . Our modeling shows that nearly all of the NO_x is NO for the conditions we are studying.

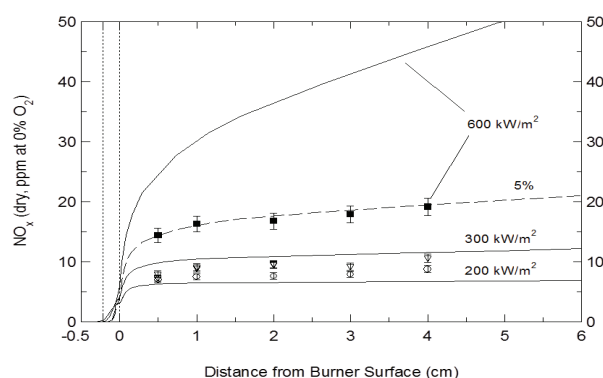


Fig. 2. Predicted and measured NO_x profiles for three firing rates at $\phi = 0.9$. Upper line and solid squares 600 kW/m^2 , blue-flame mode; middle solid line and triangles are 300 kW/m^2 , radiant mode; lower solid line and circles are 200 kW/m^2 , radiant mode. The dashed line shows the effect of decreasing the 600 kW/m^2 temperature by 5% (70-100 K) above the porous medium. The porous medium extends from -0.22 cm to 0.0 cm.

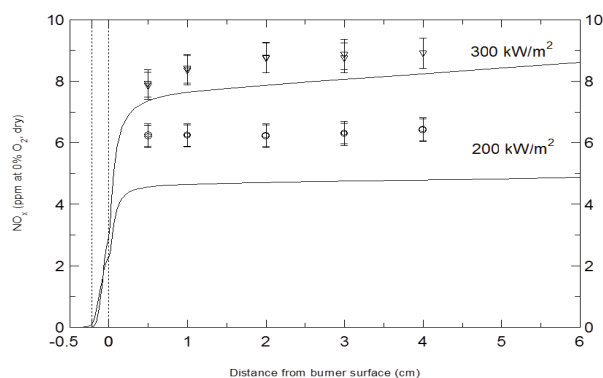


Fig. 3. Predicted and measured NO_x profiles for two firing rates at $\phi = 0.8$, full radiant mode. The upper solid line and triangles correspond to a firing rate of 300 kW/m^2 ; lower solid line and circles represent a firing rate of 200 kW/m^2 .

Table 1

Calculated maximum gas temperature, adiabatic flame temperature and radiant efficiency for flow conditions examined in this paper

Firing Rate (kW/m^2)	ϕ	Calculated Maximum Gas Temperature (K)	Calculated Adiabatic Flame Temperature (K)	Radiant Efficiency (%)
200	0.8	1652	2002	16.2
300	0.8	1740	2002	12.6
200	0.9	1693	2137	19.4
300	0.9	1775	2137	16.4
600	0.9	1961	2137	8.7

Results and Discussion

Comparison of Model and Experiment

Model predictions of NO_x concentration (translated to 0% oxygen, dry) for $\phi = 0.9$ are compared with measurements in Fig. 2. The agreement is good at lower firing rates but not at the highest firing rate. For the highest firing rate, the gas is hot enough such that the Zeldovich mechanism is active, thus the temperature of the gas is extremely important. The gas above the burner radiates heat and additional heat was lost from the porous medium to the burner housing. Calculations in which the gas temperature is artificially lowered above the burner by just 5% (70–100 K) show excellent agreement with the experiment (see the dashed line in Fig. 2). Similar magnitudes of temperature decrease have been observed experimentally in these types of burners [8, 11]. We suspect that the combination of gas radiation and heat loss to the burner housing lowered

the temperature enough to result in the discrepancy between the predicted temperature and measured temperature. Nonetheless, we can learn much from the numerical model even with this over-prediction of NO_x .

The calculated maximum gas temperatures for the surface-flame burner at $\phi = 0.9$ are 1693 K at 200 kW/m^2 , 1781 K at 300 kW/m^2 , and 1961 K at 600 kW/m^2 , as shown in Table 1. Note that the adiabatic flame temperature of a $\phi = 0.9$ methane-air flame is 2137 K, and the adiabatic flame temperature of a $\phi = 0.8$ methane-air flame is 2002 K. Thus, combustion in a surface-flame burner results in a temperature decrease between 175 and 450 K from adiabatic conditions.

Measurements and predictions for $\phi = 0.8$ are shown in Fig. 3. Agreement is fair. The deviation at the lower firing rates for both equivalence ratios is possibly caused by uncertainty in rate constants of the less-well known NO mechanisms or experimental uncertainty. Overall, the model shows good agreement with the experiments, but for higher firing rates we consider the predictions to be an upper bound.

Numerical Analysis of NO Formation Mechanisms

Calculations were performed for commonly used equivalence ratios ($\phi = 0.8$ and 0.9) and firing rates (200, 300 and 600 kW/m^2). In each figure, the porous medium extends from -0.22 to 0.0 cm. The predicted NO levels shown in the Figs. 5–7 are not translated to different oxygen or water concentrations; thus, the profiles can not be directly compared with those in Fig. 2 and 3. Note that the final mole percent of O_2 is 1.92% at $\phi = 0.9$ and 3.88% at $\phi = 0.8$. The final mole percent of H_2O is 17.3% at $\phi = 0.9$ and 15.5% at $\phi = 0.8$.

Figure 4 shows the NO profiles for a burner operating on the lower range of the blue-flame mode (600 kW/m^2 , $\phi = 0.9$). NO levels reach almost 20 ppm just past the flame front, as about 15 ppm are formed in the flame front. For this firing rate, the Zeldovich reactions are dominant and responsible for much of the NO just above the burner, which causes the NO concentration to increase steadily until the gases cool. The peak gas temperature is 1961 K, which is over 200 K lower than the adiabatic flame temperature of a $\phi = 0.9$ methane-air mixture. The heat transfer from the flame to the porous medium reduces the NO formation rate substantially, resulting in a low-NO premixed burner with high stability. The NNH, N_2O and ‘other’ pathways each contribute about 2–4 ppm of NO; the Fenimore mechanism is responsible for about 1 ppm.

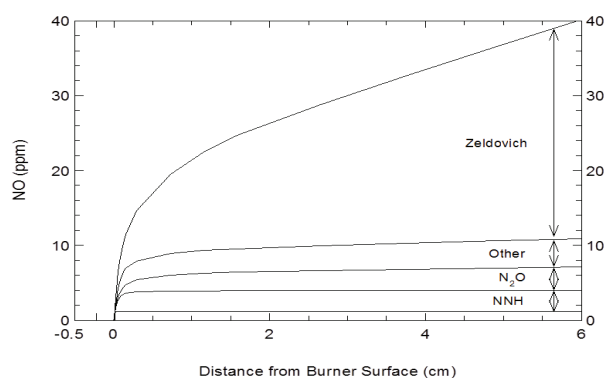


Fig. 4. NO contributions from each mechanism and the combined NO concentration. The firing rate is 600 kW/m² and $\phi = 0.9$; the burner is most likely operating in blue-flame mode. The uppermost solid line is the total NO; lower lines delineate the contribution from each mechanism. The region between the x-axis and the first curve denotes the Fenimore NO contribution. The porous medium extends from -0.5 to 0.0 cm in this figure and following figures. The peak gas temperature is 1961 K.

As we decrease the firing rate and enter the radiant mode, more heat is extracted from the flame to stabilize it on the porous medium. Since the NO formation rate is highly dependent on gas temperature, the temperature change causes a significant alteration of the NO formation pathways. Figure 5 shows NO mechanism contributions for 300 kW/m² and $\phi = 0.9$. Most of the NO is formed in the flame front through the NNH, N₂O and ‘Other’ pathways. Therefore, even if the exhaust gases are cooled immediately, at least 7 ppm of NO will be formed. Less than one-seventh of the NO is formed through the Fenimore pathway.

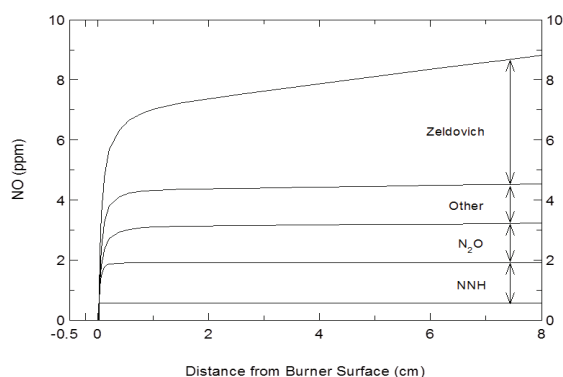


Fig. 5. NO contributions from each mechanism and the combined NO concentration. The firing rate is 300 kW/m² and $\phi = 0.9$. The uppermost solid line is the total NO; lower lines delineate the contribution from each mechanism. The region between the x-axis and the first curve denotes the Fenimore NO contribution. The peak gas temperature is 1775 K.

At the lowest firing rate (200 kW/m²) and lowest equivalence ratio ($\phi = 0.8$), non-flame-front Zeldovich NO is almost negligible and most of the NO is formed in the flame front (see Fig. 6). The contributions of flame-front Zeldovich, NNH, N₂O and ‘Other’ mechanisms are roughly equal at about 0.7 ppm each. The Fenimore mechanism is responsible for one-twelfth of the NO.

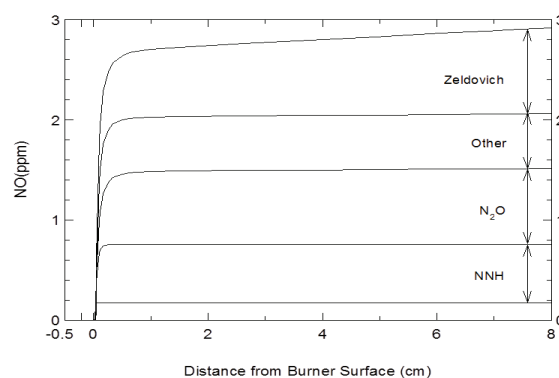


Fig. 6. NO contributions from each mechanism and the combined NO concentration. The firing rate is 200 kW/m² and $\phi = 0.8$. The uppermost solid line is the total NO; lower lines delineate the contribution from each mechanism. The region between the x-axis and the first curve denotes the Fenimore NO contribution. The peak gas temperature is 1652 K.

In the 200 and 300 kW/m² flames, Fenimore NO is the least important mechanism, with the Zeldovich and N₂O mechanisms producing the majority of the NO. This finding differs from the results of Williams et al. [11] and Sullivan and Kendall [10]. Williams et al. [11] estimated the NO production using empirical formulas and assumptions of partial equilibrium. They argued that most of the NO is formed by the Fenimore mechanism, but cautioned that their estimates were subject to “considerable errors” [11]. Sullivan and Kendall [10] determined the fraction of NO produced by the Fenimore mechanism by first calculating the NO_x with the Miller-Bowman chemical mechanism [13], then removing CH+N₂ ↔ HCN+N from the chemical mechanism and recalculating the NO_x for identical stoichiometry and flow rate. Their calculations showed that the Fenimore mechanism produces most of the NO_x at low firing rates and about 50% of the NO_x at high firing rates. To determine whether our results depend on the method of quantifying the NO formation pathways, we used Sullivan and Kendall’s method and found that the Fenimore mechanism was still responsible for less than 20% of the NO at each firing rate. Since the method of calculation has no significant

effect on our prediction of Fenimore NO production, we conclude that differences between our results and those of Sullivan and Kendall are the result of differences between the chemical mechanisms.

It should be noted that any chemical mechanism is a work-in-progress, and that numerous changes may be made as new experimental and/or modeling results become available. Indeed, recent investigations [34, 35] of the $\text{CH} + \text{N}_2 \leftrightarrow \text{HCN} + \text{N}$ reaction found that the rate used in GRI-Mech 2.11 should be increased by a factor of between 2 and 4. The authors of Ref. [34] also suggest that further study of the reaction is necessary, with consideration of both NO and CH profiles. In order to estimate the effect that mechanism modifications would have on NO formation in surface-flame burners, a sensitivity analysis is used. At each firing rate, NO production in the flame front is most sensitive to $\text{NNH} + \text{O} \leftrightarrow \text{NH} + \text{NO}$, with the next most sensitive reaction ($\text{CH} + \text{N}_2 \leftrightarrow \text{HCN} + \text{N}$) having a normalized sensitivity coefficient roughly 50% smaller. As the distance from the porous medium increases, the sensitivity of $\text{N}_2 + \text{O} \leftrightarrow \text{NO} + \text{N}$ increases, with the highest rate of increase at $q = 600 \text{ kW/m}^2$.

Presentation of NO emissions is not straightforward because NO reaches equilibrium slowly. If one presents NO vs. firing rate, for example, the slope of the curve depends on how far away from the burner the NO is sampled. This behavior is shown in Fig. 7, where emission indices for NO_x (E_{INO_x}) at two distances are presented as a function of firing rate. The E_{INO_x} is defined here as the mass of NO_x at a given distance (assuming that all NO is converted to NO_2) divided by the mass of fuel burned. The transition between radiant mode and blue-flame mode for current surface-flame burners occurs at approximately 450 kW/m^2 [36] and is shown in Fig. 7. The increase in the emission index with firing rate is more dramatic at the 10-cm plane than at the 1-cm plane. The importance of Fig. 7, though, is that it shows loose bounds for NO emissions at various firing rates for a given equivalence ratio. Since the model has no gas radiation or burner housing heat losses, the 10-cm curve shows the maximum NO emissions one can expect from the surface-flame burner. Even if the burner is housed in a location that provides instant cooling of the exhaust above the burner, the lower curve shows the NO emissions that can be expected, assuming that heat losses to the burner housing are minuscule. As the firing rate increases, the flame begins to lift off the burner, thus reducing radiant output and becoming a blue-flame mode surface-flame burner. The model considers the flame to be perfectly flat; therefore, effects of partially-lifted flames are not explicitly accounted for.

As the firing rate increases in surface-flame burners, the radiant efficiency (percent of chemical input that is emitted as thermal radiation) declines while the NO_x emission rises (see Fig. 7 and Table 1). Thus, a burner operated at a high firing rate will radiate inefficiently (possibly with a partially lifted flame) and emit *relatively* high amounts of NO_x .

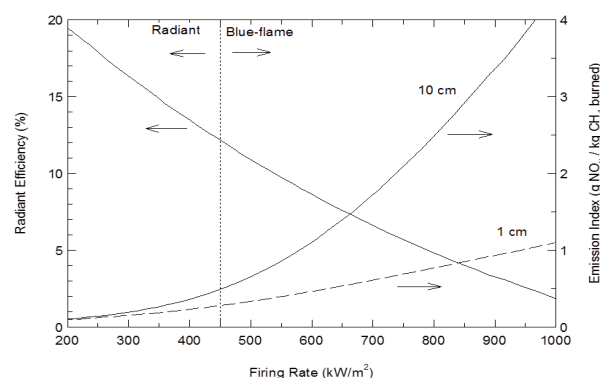


Fig. 7. Predictions of radiant efficiency and NO_x emission index ($\text{g-NO}_x/\text{kg-CH}_4$ burned) at 1 cm (dashed) and 10 cm (solid) above the burner. The 10-cm NO_x emission index should be seen as a rough upper limit because heat loss from the porous medium to the burner housing and radiation from the gas is neglected in the calculations.

Sensitivity of NO_x Emissions to Properties of the Porous Medium

To investigate the sensitivity of NO_x emissions to porous medium properties, we varied the porous medium properties for a $\phi = 0.9$ flame at firing rates of 200, 300 and 600 kW/m^2 . The following parameters were independently varied: extinction coefficient (varied from 500 to 5000 m^{-1}), scattering albedo (0.25 to 0.90), effective thermal conductivity (10^{-4} to 1 W/m-K), porosity (0.5 to 0.95) and forward scattering fraction (0.25 to 1.0). The ‘nominal’ properties were as listed in the ‘‘Properties of the Porous Medium’’ section above.

Our calculations show that the sensitivity of NO_x emission to porous medium properties is strongly dependent on firing rate. At a firing rate of 200 kW/m^2 , variation of the porous medium properties leads to no appreciable change in NO_x emission or gas temperature. At 300 kW/m^2 , variation of the properties leads to changes in NO_x of less than 10% and changes in maximum gas temperature of under 10 K (out of $\sim 1750 \text{ K}$). At 600 kW/m^2 , changes in NO_x emission were up to 25% and changes in maximum gas temperature were up to 40 K (out of $\sim 1950 \text{ K}$). Since the highly temperature sensitive Zeldovich mechanism is active at 600 kW/m^2 , small tempera-

ture changes can result in large NO_x changes. Recall Fig. 2, in which model overpredicts the NO_x emission by a factor of 2 at a firing rate of 600 kW/m^2 , whereas an extensive variation change in properties results in only about a 25% change in NO_x . Therefore, we doubt that misestimation of porous medium properties is the cause for the deviation between model and experiment in Fig. 2.

Conclusions

Surface-flame burner operation in radiant and blue-flame mode has been simulated. Since the performance of a surface-flame burner is governed by many different factors, a comprehensive model is a valuable tool to gain insight into burner operation. We measured NO_x profiles above a surface-flame burner with a metal fiber porous medium and compared the measurements with predictions. The model predicts NO_x concentration with reasonable success. Deviations between model and experiment are the result of the heat loss in the experiment and uncertainty in the chemical rate constants for some of the NO reactions.

Simulations of surface-flame burners show that Zeldovich NO is active only at high firing rates (above 600 kW/m^2 at $\phi = 0.9$), where it is responsible for 50-60% of the total NO (and increasing with height above the burner). The Zeldovich route is even more important at equivalence ratios closer to $\phi = 1.0$ and firing rates higher than 600 kW/m^2 . At high firing rates with $\phi < 0.9$, NO emissions decrease and the radiant efficiency drops rapidly. In the 200 and 300 kW/m^2 firing rate simulations, nearly all of the NO is formed in the flame front. The Zeldovich mechanism was responsible for 20-30% of the total NO, the Fenimore pathway accounts for about less than 10% of the NO, and 50-75% of the NO is formed through the NNH-path, the N_2O -path and other reactions. Sensitivity analysis shows that NO production in the flame front is most sensitive to $\text{NNH} + \text{O} = \text{NH} + \text{NO}$, with $\text{CH} + \text{N}_2 = \text{HCN} + \text{N}$ having the second highest sensitivity coefficient. Since most of the NO is formed through the non-Zeldovich route at moderate to low firing rates, any attempt to predict NO emissions from surface-flame burners should use a full chemical mechanism that includes nitrogen chemistry.

At low firing rates, properties of the porous medium have no appreciable effect on NO_x emissions. At high firing rate, NO_x emissions are slightly sensitive to porous medium properties because of the extreme sensitivity of NO_x to temperature. The sensitivity of NO_x emissions to porous medium properties, however, is small compared to the effect of heat losses by the flame and post-flame gases.

Acknowledgment

This work was supported by the Gas Research Institute. We thank Professor Raymond Viskanta of Purdue University (West Lafayette, IN), Mr. Shyam Singh of SSEI, Inc. (Rockford, IL) and Dr. Kevin Krist of GRI (Chicago, IL) for useful discussions about heat and mass transport in porous media.

References

- [1]. J. Goovaerts, K. Ratnani, and B. Hendry, *Pulp and Paper Canada* 92 (1991) 24–27.
- [2]. P. Mattsson, J. Pelkonen, A. Riikonen, and N. Oy, *Paperi ja Puu—Paper and Timber* 72 (1990) 347–349.
- [3]. S. Singh, M. Ziolkowski, J. Sultzbaugh, and R. Viskanta, in *Fossil Fuel Combustion* (R. Ruiz, Ed.), 1992, ASME PD-33, p. 111.
- [4]. F. Andersen, *Prog. Energy Comb. Sci.*, 18 (1992) 1–12.
- [5]. Y.-K. Chen, R.D. Matthews, and J.R. Howell, in *Radiation, Phase Change Heat Transfer and Thermal Systems* (Y. Jaluria et al., Ed.), 1987, ASME HTD- 81, p. 35.
- [6]. S.B. Sathe, R.E. Peck, and T.W. Tong, *Int. J. Heat Mass Transfer* 33 (1990) 1331–1338.
- [7]. P.H. Bouma, R.L.G.M. Eggels, L.M.T. Somers, L.P.H. de Goeij, J.K. Nieuwenhuizen, and A. Van Der Drift, *Combust. Sci. Technol.* 108 (1994) 193-203.
- [8]. M. Kulkarni, Ph.D. dissertation, Arizona State University, 1996.
- [9]. P.-F. Hsu, W.D. Evans, and J.R. Howell, *Combust. Sci. Technol.* 90 (1993) 149-172.
- [10]. J.D. Sullivan, and R.M. Kendall, *International Gas Research Conference*, Orlando, Florida, 1992.
- [11]. A. Williams, R. Woolley, and M. Lawes, *Combust. Flame* 89 (1992) 157–166.
- [12]. A.V. Mokhov, and H.B. Levinsky, 26th Symp. (Int.) Combust., The Combustion Institute, Pittsburgh, 1996, pp. 2147–2154.
- [13]. J.A. Miller, and C. T. Bowman, *Prog. Energ. Combust. Sci.* 15 (1989) 287–338.
- [14]. R.J. Kee, J.F. Grcar, M.D. Smooke, and J.A. Miller, (1985), A Fortran Program for Modeling Steady Laminar One-Dimensional Premixed Flames, Sandia National Laboratory, SAND85-8240.
- [15]. M.D. Rumminger, N.H. Heberle, R.W. Dibble, and D.R. Crosley, 26th Symp. (Int.) Combust., The Combustion Institute, Pittsburgh, 1996, pp. 1755–1762.
- [16]. M.D. Rumminger, Ph.D. dissertation, University of California, Berkeley, 1996.

- [17]. R.J. Kee, F.M. Rupley, and J.A. Miller, (1989), CHEMKIN-II: A Fortran Chemical Kinetics Package for the Analysis of Gas Phase Chemical Kinetics, Sandia National Laboratory, SAND89-8009B.
- [18]. R.J. Kee, G. Dixon-Lewis, G. Warnatz, M.E. Coltrin, and J.A. Miller, (1986), A Fortran Computer Package for the Evaluation of Gas-Phase, Multicomponent Transport Properties, Sandia National Laboratory, SAND86-8246.
- [19]. J.F. Grcar, (1992), The Twopnt Program for Boundary Value Problems, Sandia National Laboratory, SAND91-8230.
- [20]. M. Golombok, A. Prothero, L.C. Shirvill, and L.M. Small, *Combust. Sci. Technol.* 77 (1991) 203–223.
- [21]. R. Mital, J.P. Gore, and R. Viskanta, (1995), AIAA Paper No. 95–2036.
- [22]. W.J. Mantle, and W.S. Chang, *J. Thermophys. Heat Transfer* 5 (1991) 545–549.
- [23]. M.G. Semena, and V.K. Zaripov, *Thermal Engineering* 24 (4) (1977) 69–72.
- [24]. R.M. Kendall, S.T. DesJardin, J.D. Sullivan, (1992), Basic Research on Radiant Burners, Gas Research Institute Report number 92-7027-171.
- [25]. S. Yagi, D. Kunii, and N. Wakao, *AIChE J.* 6 (1960) 543–546.
- [26]. C.T. Bowman, R.K. Hanson, W.C. Gardiner, V. Lissianski, M. Frenklach, M. Goldenberg and G.P. Smith, “GRI-Mech 2.11 - An Optimized Detailed Chemical Reaction mechanism for Methane Combustion and NO Formation and Reburning,” GRI-Report GRI-97/0020, March 1997.
- [27]. Y.B. Zeldovich, *Acta Physiocochemica USSR*, 21: 577 (1946).
- [28]. C.P. Fenimore, 13th Symp. (Int.) on Combust., The Combustion Institute, Pittsburgh, 1970, pp. 373–380.
- [29]. J. Wolfrum, *Chemie Ingenieur Technik*, 44: 656 (1972).
- [30]. P.C. Malte, and D.T. Pratt, *Combust. Sci. Tech.*, 9:221 (1974).
- [31]. J.W. Bozzelli, and A.M. Dean, *Int. J. Chem. Kinet.* 27 (1995) 1097–1109.
- [32]. R.C. Flagan, and J.H. Seinfeld, *Fundamentals of Air Pollution Engineering*. Prentice-Hall, Inc., Englewood Cliffs, NJ, 1988.
- [33]. A. Schlegel, S. Buser, P. Benz, H. Bockhorn, and F. Mauss, 25th Symp. (Int.) on Combust., The Combustion Institute, Pittsburgh, 1994, pp. 1019–1026.
- [34]. P.A. Berg, G.P. Smith, J.B. Jeffries, and D.R. Crosley, 27th Symp. (Int.) on Combust., The Combustion Institute, Pittsburgh, 1998, pp. 1377–1384.
- [35]. V. Sick, F. Hildenbrand, and P. Lindstedt, 27th Symp. (Int.) on Combust., The Combustion Institute, Pittsburgh, 1998, pp. 1401–1409.
- [36]. S. Singh, Personal communication, January 1996.

Received 11 March 2014